Effects of SiO$_2$ Contaminant on Thermo-Mechanical/Chemical Properties and Lubricity of PFPE Lubricants

Shahriar Rahman [1], Dipesh Purani [2], Shaikh Ali [2] and Chang-Dong Yeo [1,*]

1   Department of Mechanical Engineering, Texas Tech University, Lubbock, TX 79409, USA;
     Shahriar.Rahman@ttu.edu
2   Seagate Technology, Shakopee, MN 55379, USA; Dipesh.Purani@seagate.com (D.P.);
     shaikh.m.ali@seagate.com (S.A.)
*   Correspondence: changdong.yeo@ttu.edu; Tel.: +1-806-834-5452

Abstract: Using the molecular dynamics (MD) simulations with ReaxFF potential, two different types of PFPE lubricants (Ztetraol and ZTMD) are prepared on a-C film, and SiO$_2$ particles are adsorbed onto the lubricants at room temperature. From the simulation results, it is observed that the adsorbed SiO$_2$ particles increase the stiffness of PFPE lubricants leading to less airshear displacement. Since Ztetraol has higher mobility with lower viscosity than ZTMD, the adsorbed SiO$_2$ particles penetrate deeper into the Ztetraol lubricants. Accordingly, the effect of SiO$_2$ on the airshear displacement is more obvious to Ztetraol than ZTMD. In addition, the adsorbed SiO$_2$ particles increase the friction force and the amount of lubricant pick-up during the sliding contact with a nanosized a-C tip.

1. Introduction

In the magnetic storage industry, achieving a higher areal recording density demands lower head-media-spacing (HMS). Under such a low HMS budget, the head surface contamination can cause fatal errors and failures during the reading and writing operation of hard disk drives (HDDs). Contaminants on a head slider surface, both organic and inorganic, can be from the disk lubricant, seals, adhesives, bearing greases or they can be airborne particles depending on the HDD operating conditions [1–3]. In recent HDD designs, as the HMS budget is reduced to a few nanometers, a common type of head surface contaminant is the transferred lubricants from the disk surface during head disk interface (HDI) interactions [4–7]. Ambekar et al. [4] experimentally and numerically investigated the effect of lubricant thickness, type, and air bearing surface design on the transfer of lubricant from disk to the head side. They reported that this lubricant transfer can occur even when the disk and the head are not in physical contact. Ma et al. [5] have found that the slider air baring pressure does not affect the lubricant transfer, rather the molecular weight of the lubricants is the dominant factor. Seo et al. [8] and Sonoda et al. [9] studied the presence of hydrocarbons in the lubricants at the head disk interface (HDI). They claimed that the presence of these contaminants and foreign particles inside HDDs can accelerate the lubricant transfer process. For these reasons, researchers have investigated the contamination of the air-bearing-surface (ABS) of a head slider through experiments and numerical simulations [8–14]. Various approaches were proposed to describe the mechanisms on how lubricants are transferred and picked up to a head surface, which includes the process of material evaporation, desorption, condensation, and molecular interaction in the HDI.

Z-type perfluoropolyether (PFPE) has been typically used as a disk lubricant in HDDs. It possesses beneficial characteristics as a lubricant such as high chemical inertness, protection against material oxidation, low volatility and vapor pressure, the ability to withstand wide range of temperature, the ability to be applied as molecularly thin layers, and high

thermal stability [15–17]. Its design adaptability enables it to be applied for other applications, including automotive applications, metal cutting, space applications, oil and gas industries, electronic industries, sheet metal forming industries, etc. [18–25]. A single PFPE lubricant chain is composed of backbone and functional end groups. It is known that functional end groups are usually anchored to the underlying solid substrate surface through the high polar interactive force. Accordingly, this helps to prevent direct solid-to-solid contact during operation, thereby reducing the wear and friction of the contacting surfaces. The long backbone is relatively softer providing the mobility of the PFPE lubricant.

Ztetraol has long been applied to a magnetic recording disk as a lubricant, which is made of Fomblin backbone with four hydroxyl (-OH) end groups. Recently, to cope with the design requirement of smaller HMS, various types of PFPE lubricants have been studied and proposed (called a low-profile lubricant (LPL)), including D4OH, TA-30, QA-40, and Ztetraol multidentate (ZTMD) [26,27]. D4OH is built upon a Demnum backbone with a similar end group structure to Ztetraol. ZTMD is an extension of Ztetraol in which the additional four -OH end groups (total of eight -OH end groups) are bonded to a Fomblin backbone in the middle of the chain [27]. This improves the film stability and conformation of the lubricant. Additionally, TA-30 and similar branched PFPE lubricants have been developed by modifying their backbone structure to increase their functionality and thermal stability [27]. These LPLs can reduce the lubricant thickness without sacrificing the lubricity significantly. However, under a flying height of a few nanometers, they can also contaminate a head slider surface due to the intermittent HDI contact. As described above, several works have been conducted previously to study the interaction of lubricants at the HDI. Lofti et al. [28] used the ReaxFF reactive forcefield to simulate the degradation of PFPE lubricants in the presence of oxygen, water, and oxide nanoparticles [28]. However, the effect of SiO_2 on both the HDI interaction and lubricant transfer from the disk to head side using a reactive forcefield has not been reported yet.

In this study, we investigate the effects of SiO_2 contaminant on the thermo-chemical/mechanical properties and lubricity of Ztetraol and ZTMD lubricants through molecular dynamics (MD) [29] simulations with ReaxFF potential. Systematic MD simulations enable a quantitative measurement of the airshear response, friction force, and material transfer (or lubricant pick-up) of SiO_2-contaminated lubricants, whose results are compared with those of non-contaminated lubricants. The research outcomes can contribute to obtaining more scientific insights into the fundamental mechanism of head surface contamination and friction during HDI interactions.

2. Methods

### 2.1. ReaxFF Force Field-Based Potential

We employ Large-scale Atomic/Molecular Massively Parallel Simulator (LAMMPS) for MD simulations [30]. The ReaxFF interatomic potential (the details are in Appendix A) is used because it can describe the chemical bonding of materials efficiently eliminating expensive calculations of quantum mechanics [31]. The ReaxFF forcefield parameters developed by Chipara et al. [32], Srinivasan et al. [33], and Chenoweth et al. [34] are applied to account for interactions among PFPE lubricants, SiO_2 particles, and a-C surface.

2.2. Material Preparation and Modeling in MD

Based on the material characterization results for a contaminated head surface in actual HDD products [35], a silicon dioxide (SiO_2) particle is selected as an HDI contaminant, and its interactions with PFPE lubricants (i.e., Ztetraol and ZTMD) and a-C surface are investigated in this study.

Figure 1 shows the preparation of SiO_2-contaminated PFPE lubricant on a-C film surface. In Figure 1b, the upper and lower a-C films are prepared using the liquid quenching method [36] with the dimension of 100 Å (W) $\times$ 100 Å (L) $\times$ 20 Å (H), which contains a total of 22,063 carbon atoms with a density of 2.2 g/cm^3. The lubricant thickness is ~13 Å for both Ztetraol and ZTMD. A single chain of lubricant is prepared using Materials

Studio (BIOVIA Materials Studio by Dassault Systems®), which is imported into visual molecular dynamics (VMD) tool. The chemical formulas of Ztetraol and ZTMD used in this MD simulation are described in Figure 1a. A single Ztetraol chain contains 169 atoms (m/n = 10/15) with four hydroxyl functional (-OH) end groups, whereas a single ZTMD chain consists of 203 atoms (m/n = 4/6). The details of the two lubricant chains are summarized in Table 1. These molecular weights agree well with those used previously in experimental work.
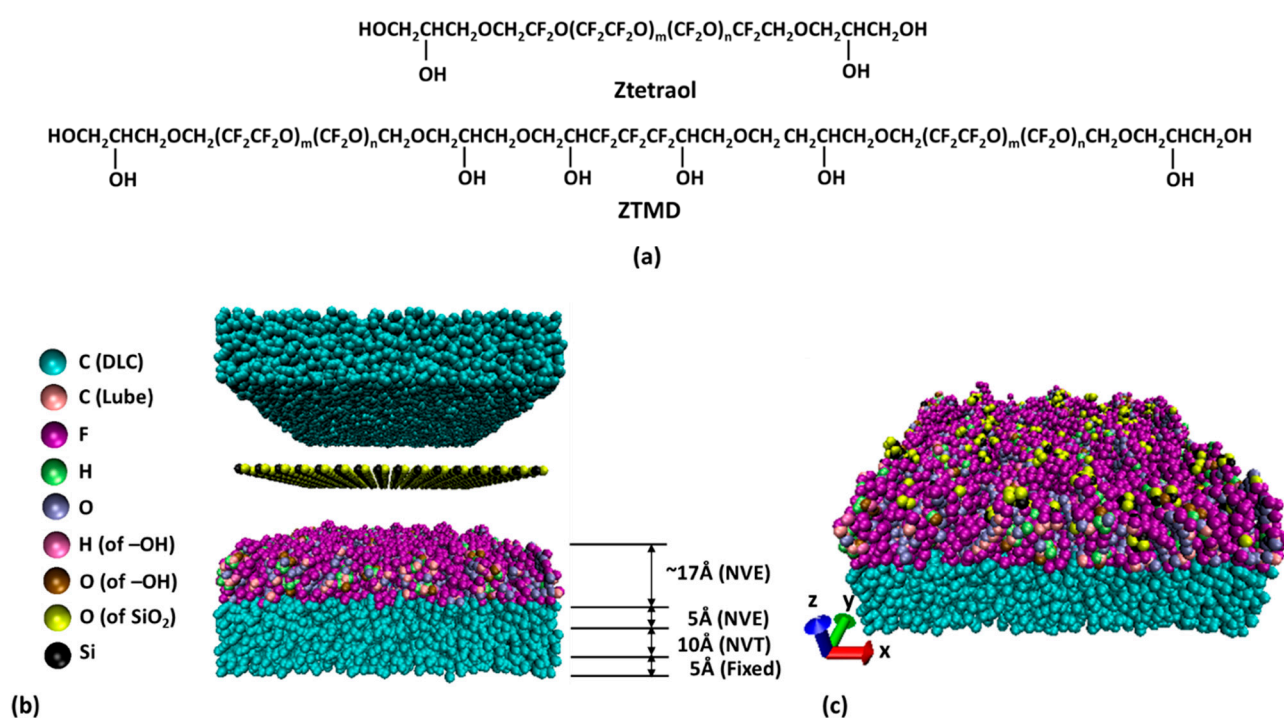
Figure 1. Preparation of SiO_2-contaminated PFPE lubricant: (**a**) chemical structures of Ztetraol and ZTMD lubricants used in the simulation, (**b**) A layer of SiO_2 contaminants placed between the top DLC and the lubricated disk before the equilibration process, and (**c**) the SiO_2 contaminated Ztetraol lubricant on a-C film.

**Table 1.** Details of a single chain of Ztetraol and ZTMD lubricants.

	Ztetraol	ZTMD
# of atoms/chain	169	203
m/n value	10/15	4/6
MW (g/mol)	2476	2608

Using the VMD's replication function, multiple lubricant chains are created in the x, y, and z directions. The as-prepared lubricant layer is brought close to the bottom a-C surface, and then the system is equilibrated at 300 K so that the lubricant layer is stabilized and settled on the bottom a-C surface. Similarly, the SiO_2 contaminants are prepared using Materials Studio and VMD's replication technique. To spread them uniformly over the lubricant's surface, a layer of SiO_2 containing a total of 256 SiO_2 particles (same size as the a-C film surface) is placed at the middle of the gap between the top a-C and the lower lubricant surfaces (Figure 1b). The bottom a-C film is divided into three layers, i.e., a fixed layer, a thermostat (NVT) layer, and a free layer with NVE ensemble. The lubricants and SiO_2 particles are free to move and interact with neighboring atoms, by which they can be stabilized (or equilibrated) with the elapsed simulation time. Periodic boundary condition is applied to x and y directions, respectively. Lastly, SiO_2 particles are adsorbed to the lubricants through the equilibration process at a controlled temperature. It is noted that the top a-C film is introduced just to prevent the SiO_2 particles from flying

off the simulation box during the equilibration process. Figure 1c shows the resulting contaminated Ztetraol lubricant after applying a layer of SiO$_2$ contaminants. Then, three more SiO$_2$ layers were introduced into the simulation box consecutively in a similar way. Once the system is equilibrated, the top a-C film is removed, and the bottom part was used for the following simulations. The SiO$_2$-contaminated ZTMD lubricant is also prepared using the same method.

2.3. Airshear Simulation

The mechanical/chemical property (i.e., stiffness and viscosity) of Ztetraol and ZTMD lubricants on a-C film is evaluated through airshear simulation. To mimic the actual airshear condition in the HDI, external force (or stress) is applied to the upper lubricants (i.e., one third lubricant layer thickness) in both normal and tangential directions, as shown in Figure 2. To measure and compare the airshear-driven lubricant displacement quantitatively, the applied stress is adjusted to $\sigma_z = 60$ MPa and $\tau_{xy} = 300$ MPa, which are higher than the actual airshear stresses [37]. The airshear simulation is carried out at 300 K, and the results are compared between Ztetraol and ZTMD lubricants with and without SiO$_2$ contamination.
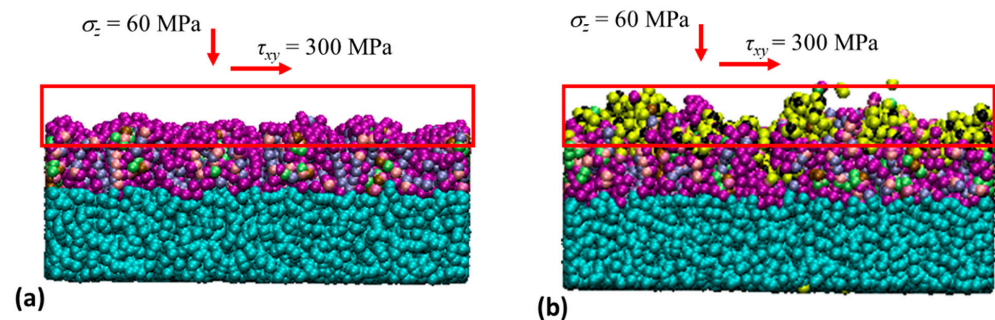
Figure 2. Scheme of the airshear simulation (**a**) without, and (**b**) with SiO$_2$ contaminants.

2.4. Sliding Contact Simulation: Friction and Lubricant Pick-Up

As shown in Figure 3, a cylindrical a-C tip with the hemispherical tip radius of 5 Å is approached to the lubricant surface with the speed of 0.2 Å/ps. At the specified tip penetration, the a-C tip makes a sliding contact with the speed of 0.4 Å/ps, from which we measure the friction force. The sliding contact speed is selected based on the actual HDD products. After finishing the sliding contact, the a-C tip is retracted upward with the speed of 0.4 Å/ps, and then the amount of materials picked up (lubricant and SiO$_2$ particles) is quantified. This sliding contact simulation is also performed at a room temperature of 300 K, and results are compared between Ztetraol and ZTMD lubricants with and without SiO$_2$ contamination.
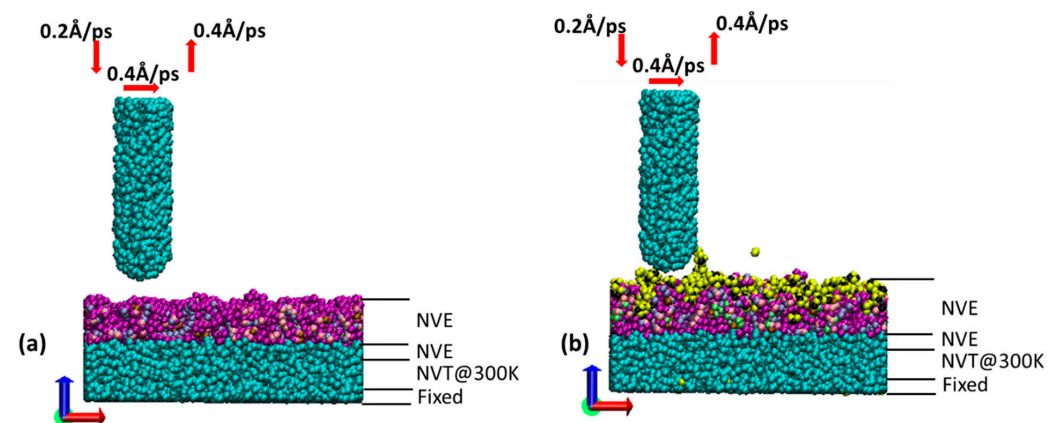

Figure 3. Scheme of the sliding contact simulation (**a**) without, and (**b**) with SiO$_2$ contaminants.

3. Results and Discussion

### 3.1. Adsorption of SiO_2 Contaminants to Ztetraol and ZTMD Lubricants

In Figure 1, the deposition of the first SiO_2 layer is shown. Then, it was followed by applying three more SiO_2 layers consecutively in a similar fashion, which were adsorbed to the lubricants through the equilibration process. Figure 4 summarizes the simulation results of SiO_2 adsorption. For both Ztetraol and ZTMD in Figure 4a, the amount of adsorbed SiO_2 particles increases with the number of supplied SiO_2 layers. When the first layer of SiO_2 particles is applied, Ztetraol shows slightly more SiO_2 adsorption than ZTMD. In the following application of SiO_2 layers, the difference in the SiO_2 adsorption between Ztetraol and ZTMD becomes larger, because the applied SiO_2 particles have a higher bonding preference to the previously adsorbed SiO_2 on the lubricants than to the lubricant atoms. Due to this bonding preference, the adsorbed SiO_2 particles are agglomerated to a bigger size with the addition of SiO_2 layers in Figure 4b.
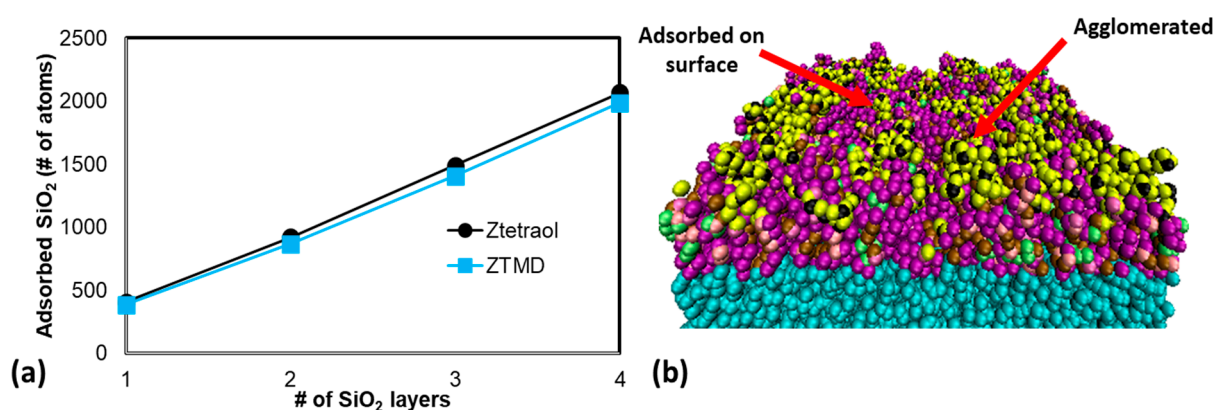
Figure 4. Adsorption of SiO_2 to Ztetraol and ZTMD: (**a**) the amount of adsorbed SiO_2 with the addition of SiO_2 layers; (**b**) the growth and agglomeration of SiO_2 particles in the lubricant.

To better visualize the molecular interactions of SiO_2 particles with the lubricants (Ztetraol and ZTMD) and the underlying a-C, the lubricant atoms are removed, thereby showing the position of the adsorbed SiO_2 within the lubricant layer on the a-C, as shown in Figure 5.

Both Ztetraol and ZTMD show more adsorbed SiO_2 with the addition of SiO_2 layers, which is consistent with the results of Figure 4a. For Ztetraol, the SiO_2 contaminants are initially adsorbed onto the lubricant surface, and then they penetrate deeper into the lubricant layer, reaching the underlying a-C surface. However, for the case of ZTMD, the adsorbed SiO_2 hardly penetrates the lower layer of lubricant, and only a few SiO_2 particles reach the underlying a-C surface. This can be attributed to the lubricant design and its ability to interact with the underlying a-C surface. As seen in Figure 1a, compared to Ztetraol with four -OH end groups, ZTMD has eight -OH end groups, which make the lubricant bond strongly to the neighboring lubricants as well as the underlying a-C surface through the polar interaction. Accordingly, ZTMD becomes stiffer than Ztetraol, and it forms a stronger bonded layer (i.e., the lower lubricant layer that consists of more -OH end groups anchored onto the a-C surface). For this reason, the adsorbed SiO_2 particles make less and a slower penetration through ZTMD than Ztetraol.
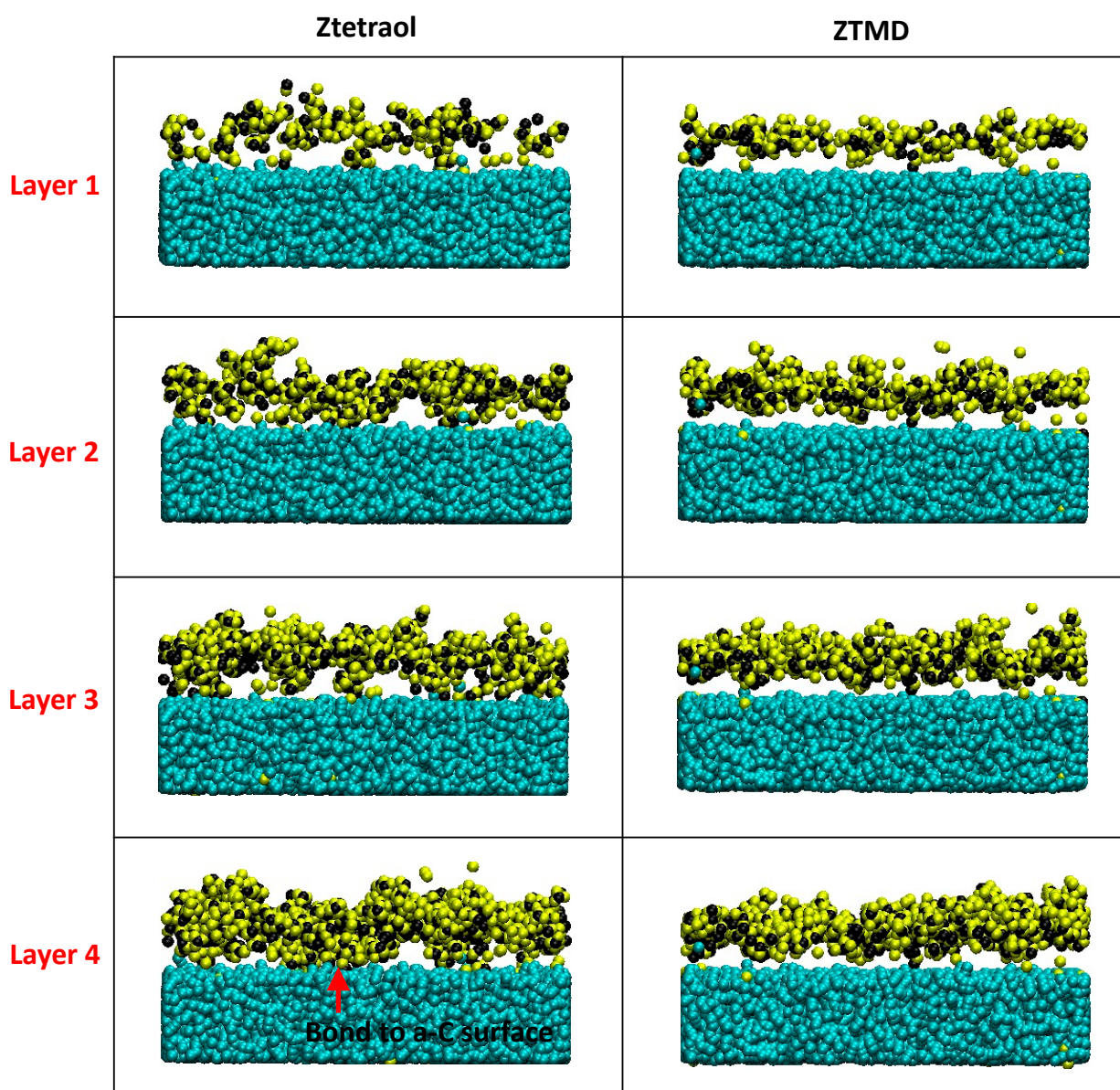
Figure 5. Comparison of SiO₂ adsorption behaviors between Ztetraol and ZTMD. The lubricant atoms are intentionally eliminated to efficiently visualize the movement and interaction of SiO₂ particles within the lubricant layer.

3.2. Measurement of Airshear Displacement

Once the four layers of SiO₂ are adsorbed onto the lubricant, the normal and shear stresses are applied to the lubricant to simulate its airshear behaviors, as seen in Figure 2. To compare the airshear-driven lubricant displacement quantitatively, we divide the lubricant into two layers, as seen in Figure 6a, the lower half (i.e., called a bonded layer, layer one) and the upper half (i.e., called a mobile layer, layer two) layer, and measure the average movement of the atoms in the (+)ve *x*-direction. Figure 6b summarizes the resulting airshear movement for the two lubricant designs, Ztetraol and ZTMD, with the different levels of SiO₂ contaminations (i.e., L0~L4 corresponding to the number of SiO₂ layers applied). Firstly, under the non-contaminated condition (i.e., L0), Ztetraol shows a significant airshear movement of 4.9 Å, which is more than two times the ZTMD airshear movement of 2.2 Å. Due to the higher stiffness and the stronger bonding to the underlying a-C surface, ZTMD is less sensitive to the applied shear stress. For both lubricant designs, the airshear movement is mostly driven by the mobile layer. Considering the bonding mechanism of a PFPE lubricant on a-C film, the bonded layer is governed by the -OH end groups anchored to the

a-C surface, while the mobile layer is dominated by the backbone materials. For this reason, the mobile layer becomes softer than the bonded layer, which accordingly results in more airshear movement. Next, when the lubricants are contaminated by SiO_2 particles, the shear displacement decreases for both Ztetraol and ZTMD. The more SiO_2 contamination of the lubricant there is, the less shear displacement there is. Since the adsorbed SiO_2 particles are interacting more with the mobile lubricant layer than the bonded lubricant layer, as seen in Figure 5, the decreasing trend of shear displacement with SiO_2 contamination in Figure 6b is mostly driven by the mobile layer (layer 2). Comparing the results between the non-contaminated and SiO_2-contaminated (L4) lubricant, the shear displacement of the mobile layer is reduced by 63 and 54% for Ztetraol and ZTMD, respectively. This implies that, on the contrary to water molecules as a contaminant in a PFPE lubricant (i.e., water molecules degrade PFPE lubricants, increasing the desorption rate and mobility), SiO_2 particles bond to the lubricants more strongly, which causes the whole lubricant layer to be stiffer than the non-contaminated lubricant, thereby leading to the smaller airshear movement. Since the non-contaminated ZTMD is sufficiently stiff and viscous, the impact of SiO_2 contamination become more obvious to Ztetraol.
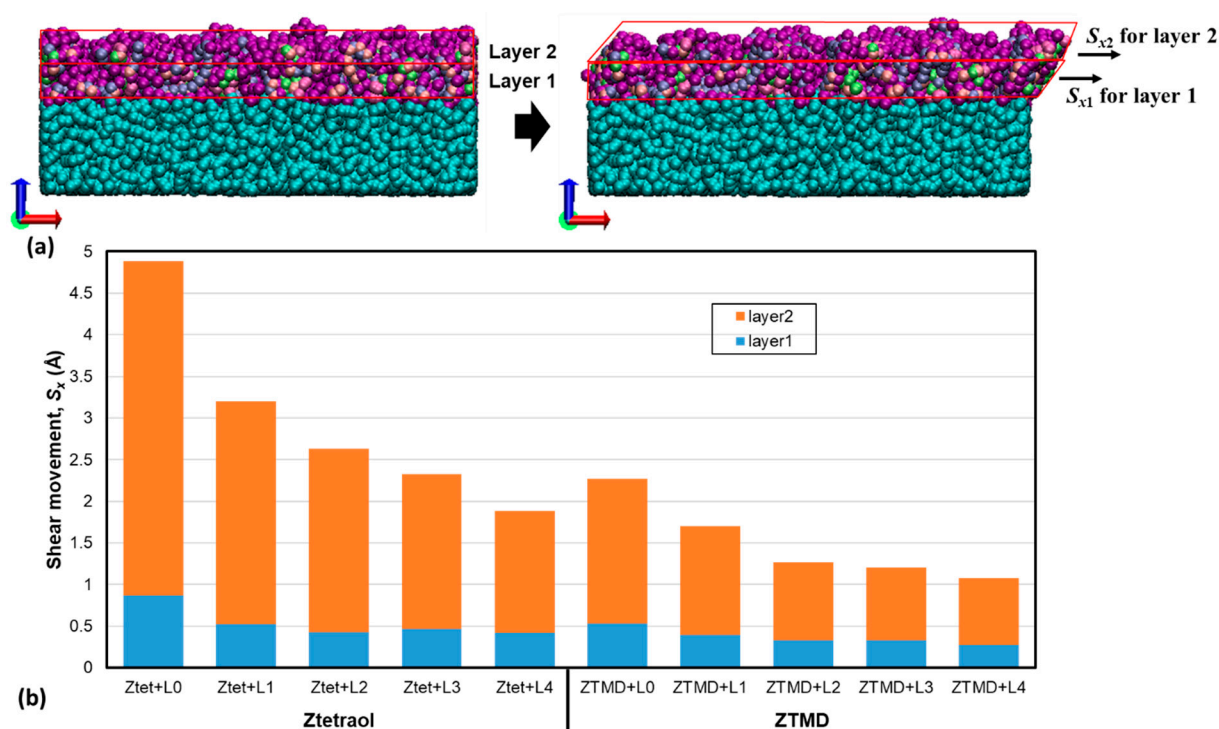
Figure 6. Results of airshear simulation for Ztetraol and ZTMD with SiO_2 contamination: (**a**) schemes to measure the airshear-driven lubricant displacement. Layers 1 and 2 represent the bonded and mobile layer, respectively; (**b**) the resulting shear displacement with the different levels of SiO_2 contaminations.

3.3. Friction Force (F_x) of Lubricants during the Sliding Contact with the a-C Tip

Using the sliding contact scheme in Figure 3, the friction force is measured with respect to the tip penetration. Figure 7 summarizes the resulting friction force for Ztetraol and ZTMD with and without SiO_2 contamination, where the tip penetration (h^*) in z-axis is normalized by the lubricant thickness. To avoid the complication of data analysis by the direct solid-to-solid contact between the a-C tip and the underlying a-C film, the tip penetration is controlled to bring it into contact with the lubricant only.
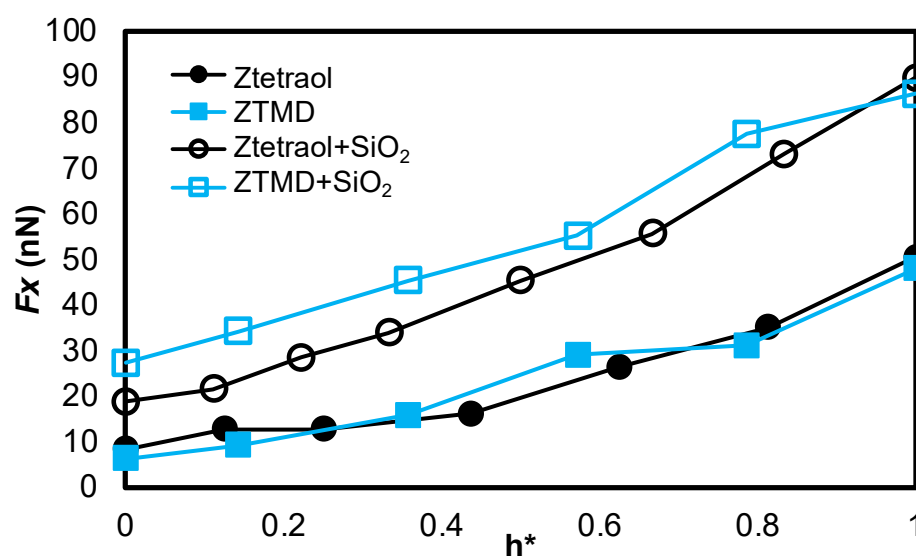
Figure 7. The measured friction force (F_x) with respect to the tip penetration for Ztetraol and ZTMD with and without SiO_2 contamination.

Firstly, under the non-contamination condition, the friction force increases with the tip penetration. Comparing the friction force between the two lubricant designs, it is observed that even though ZTMD is stiffer than Ztetraol, their friction force values are not much different. This can be explained by the friction mechanism between the tip and the lubricant. When the a-C tip slides over the lubricant, the resulting friction force can be affected more by the molecular interaction between the lubricant chains and the a-C tip surface than the lubricant's bulk property itself (i.e., viscosity). Figure 8 shows the images captured of the sliding contact simulation for Ztetraol. During the sliding contact, the lubricant chains (red- and yellow-colored atoms) are brought to bond to the a-C tip surface (Figure 8a), which resist the tip sliding movement, thereby increasing the friction force. At the further tip sliding, the bonded lubricant chains are broken (Figure 8b), which results in the decrease in friction force. Considering Ztetraol and ZTMD are made of the same Fomblin backbone, the force to break the lubricant chain might not be much different, which could result in their comparable friction force during the sliding contact.
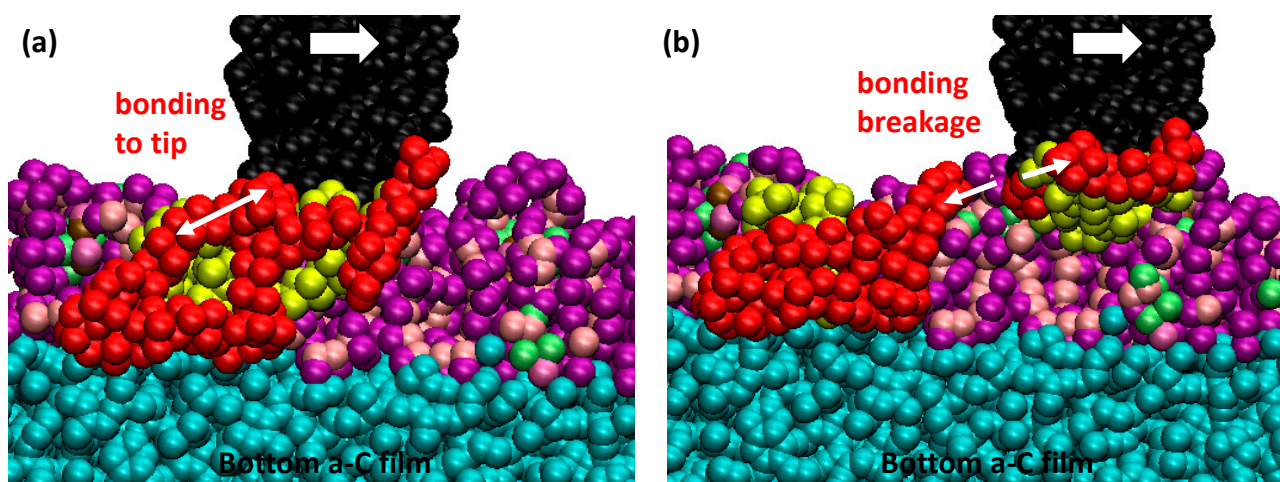
Figure 8. Friction mechanism during the a-C tip sliding contact: (**a**) the red-/yellow-colored lubricant chains bonded to the a-C tip surface are holding and resisting the tip movement (i.e., generating the friction force) and then (**b**) they are broken at the further sliding movement. It is noted that the red and yellow colors are manually assigned to better visualize the molecular interactions between the lubricant chains and the a-C tip surface.

Next, for the case of SiO_2-contamination, both lubricant designs show a significantly higher friction force than the values in the non-contaminated condition. From the results of SiO_2 adsorption and airshear simulation in Figures 4–6, it is found that SiO_2 particles make a strong bond to themselves (i.e., agglomeration) as well as to the neighboring lubricant. This indicates that the friction under the SiO_2 contamination can be determined by the molecular interactions among the sliding a-C tip surface, SiO_2, and lubricant. Based on the sliding contact simulation results, it is observed that when the a-C tip approaches and slides over the lubricated disk, the SiO_2 particles on the lubricant surface are quickly bonded to the interacting a-C tip surface, and then the neighboring lubricant chains are attracted to those SiO_2 particles on the a-C tip surface. The details of the material transfer process during the sliding contact are described in the following section. Compared to the non-contaminated condition, the SiO_2-contaminated a-C tip pulls and drags more lubricant chains during the sliding contact, which accordingly results in higher friction force. The more SiO_2 particles that are bonded to the a-C tip, the higher the friction force is. Additionally, under the SiO_2 contamination, ZTMD shows a higher friction force than Ztetraol, except at $h^* = 1$. As seen in Figure 5, since the SiO_2 particles hardly penetrate the bonded layer of ZTMD, they are more likely to be located on the surface to mid-layer of the lubricant. For this reason, when the a-C tip slides over the contaminated ZTMD, more SiO_2 particles are bonded to the a-C tip surface, which leads to a higher friction force than the contaminated Ztetraol. At the deep tip penetration at $h^* = 1$, the sliding a-C tip end interacts less with SiO_2 particles for ZTMD, thereby leading to slightly lower friction than Ztetraol.

3.4. Material Transfer and Pick-Up Behavior

After the a-C tip finishes the sliding contact over the distance of 40 Å in Section 3.3, it is retracted upward to evaluate the number of transferred lubricants and SiO_2 contaminants to the a-C tip surface. In this study, we count the total number of transferred atoms to the a-C tip surface at each tip penetration, which are summarized in Figure 9.

First, under the non-contaminated condition, the two lubricant designs do not show a significant difference at the tip penetration of $h^* = 0\sim0.6$, where both lubricant designs show the increasing trend of lubricant pick-up with the tip penetration. However, at the deeper tip penetration of $h^* = 0.8\sim1.0$, the amount of lubricant pick-up continuously increases with the tip penetration for Ztetraol, but it does not change much for ZTMD. This can be explained by the lubricant design of ZTMD and its interactions with the underlying a-C film and the sliding a-C tip. As discussed in Section 3.2, ZTMD forms a stiffer and stronger bonded layer than Ztetraol, because more -OH end groups are anchored to the underlying a-C film surface. Therefore, even if the a-C tip penetrates and slides through ZTMD's bonded layer, the lubricant atoms in the bonded layer may not be picked up easily due to their stronger bond with the underlying a-C film surface.

Next, for the SiO_2-contaminated lubricants, the overall trend of material pick-up with the tip penetration is similar, but it shows more material pick-up than the non-contaminated lubricants. The material transfer or pick-up process is dominated by the SiO_2 contaminants in the lubricant, the same as the friction mechanism. Since the SiO_2-contaminated a-C tip attracts and drags more neighboring lubricant chains during the sliding contact, it produces a larger amount of material pick-up than the non-contaminated lubricants after the tip retraction. Both lubricant designs basically show more material pick-up at the deeper tip penetration because it enables more interactions of the a-C tip surface with SiO_2 particles and the lubricant. For example, when the a-C tip makes a sliding contact with the SiO_2-contaminated Ztetraol at the deeper penetration of $h^* = 0.8$ (point A in Figure 8b), more SiO_2 particles in the lubricant are attracted and bond to the a-C tip surface. Then, during the tip retraction process, the strongly bonded SiO_2 particles on the a-C tip surface pull the adjacent interacting lubricant molecules together, which results in more material pick-up at the further tip retraction. In the case of SiO_2-contaminated ZTMD, the amount of material pick-up shows an increasing trend at the tip penetration of $h^* = 0\sim0.6$, but it

decreases after the tip penetration of $h^* = 0.8$. From the analysis of the MD simulation results in terms of material interactions (point B in Figure 9b), it is observed that during the sliding contact, the lubricant molecules are piled up in the leading edge of the a-C tip (red-dashed circles), which prevents the a-C tip surface interacting with the SiO_2 particles in the lubricant. Accordingly, at the moment of the tip retraction process, a smaller number of SiO_2 particles are bonded to the a-C tip surface, thereby leading to less material pick-up.
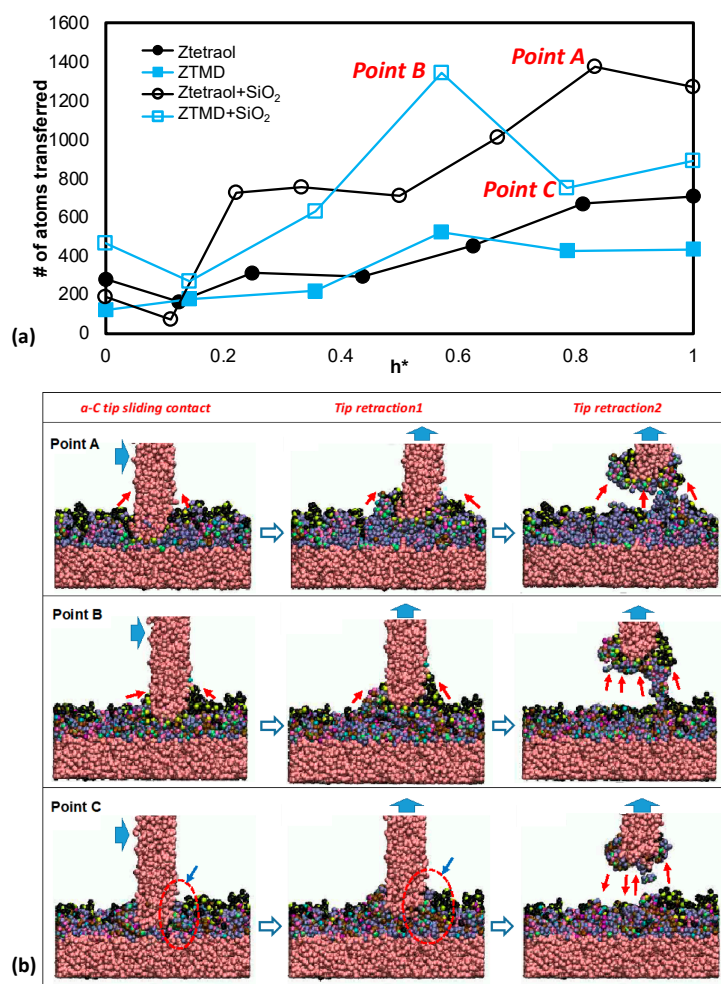
Figure 9. Results of material transfer to the a-C tip after the sliding contact: (**a**) The number of transferred atoms with respect to the tip penetration for Ztetraol and ZTMD with and without SiO_2 contamination, and (**b**) Mechanism of material transfer and pick-up for the contaminated lubricants—point A for Ztetraol at $h^* = 0.8$, point B for ZTMD at $h^* = 0.6$, and point C for ZTMD at $h^* = 0.8$.

Figure 10 shows the images of the fully retracted a-C tip after the sliding contact for both Ztetraol and ZTMD. To better visualize the bonding process of SiO_2 particles and lubricant atoms to the a-C tip surface, the a-C tips are compared with and without lubricant atoms. It is found that the a-C tip surface is mostly covered by the SiO_2 particles, under which the lubricant atoms are adhered or hanging. In other words, instead of directly bonding to the a-C tip surface, the lubricant atoms are bonded to and picked up by those underlying SiO_2 particles. This result supports the mechanism of friction force and material pick-up for the SiO_2-contaminated lubricants as described above.
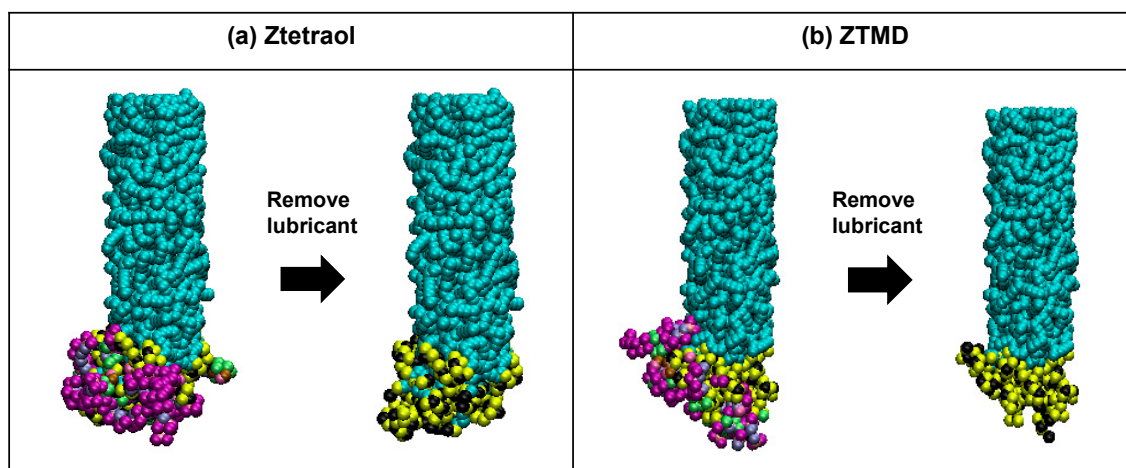
Figure 10. Process of materials bonding to and picked up by the a-C tip for (**a**) Ztetraol and (**b**) ZTMD under SiO_2 contamination.

4. Conclusions

Based on the material characterization results for a contaminated head surface in actual HDDs, the SiO_2 particle is selected as a contaminant in this study. Using the MD simulation with the ReaxFF potential, SiO_2 particles are adsorbed onto Ztetraol and ZTMD. The airshear simulation results show that, on the contrary to water molecule as an HDI contaminant (i.e., increasing the desorption rate and mobility of the PFPE lubricant), the SiO_2 particles increase the stiffness of PFPE lubricants, leading to less airshear displacement than non-contaminated lubricants. Since the adsorbed SiO_2 particles penetrate deeper into Ztetraol due to its lower stiffness, the effect of SiO_2 on airshear displacement is more obvious to Ztetraol than ZTMD. From the sliding contact simulation results, it is found that the adsorbed SiO_2 particles increase the friction force and the amount of material pick-up. Considering the SiO_2-contaminated tip attracts and drags more lubricant chains during the sliding contact, it requires a higher tangential force to keep the sliding motion and pulls up a higher number of materials at the moment of tip retraction. Therefore, from those MD simulation results, it is evident that if SiO_2 particles are not controlled properly, they can increase the HDI friction and exacerbate the head surface contamination, leading to fatal tribological failures during HDD operation.

Appendix A

In this work, a ReaxFF/reactive forcefield has been used to perform the MD simulation. ReaxFF is a bond-order-based reactive forcefield where both bond formation and dissociation are taken into consideration when the system is going through MD simulation. This technique calculates the bond order between each atom pair, which is updated in every timestep. This enables a reasonable transition from nonbonded to other possible bonded states (i.e., single, double, and triple bonds). It provides accurate simulation results of chemical reactions equivalent to quantum mechanics solutions while reducing the computational cost a lot. Here, each element present in the simulation is designated by a single tom time and prior knowledge of either connectivity information or reaction site is not needed. The total system energy calculated by this forcefield is as follows:

$$E_{system} = E_{bond} + E_{over} + E_{under} + E_{tor} + E_{val} + E_{lp} + E_{vdw} + E_{coulombic} \qquad (A1)$$

It appears that this forcefield considers both bonded (i.e., covalent) and non-bonded interaction between the respective atoms. Here, bond energy (E_{bond}), over-coordination (E_{over}), and under-coordination (E_{under}) are the bond order dependent contributions to the total energy; torsion angle energy (E_{tor}), valence-angle energy (E_{val}), and lone pair energy (E_{lp}) are the associated energy penalty terms; and van der Waals (E_{vdw}) and Coulomb energy ($E_{coulomb}$) are the non-bonded energy terms. All the connectivity terms are dependent on the bond order, while non-bonded terms are considered for every atom pair in the system. The electronegativity equalization method (EEM) is utilized to calculate the changing charge terms in each atom [38].

References

1. Nebenzahl, L.; Nagarajan, R.; Wong, J.; Volpe, L.; Whitney, G. Chemical Integration and Contamination Control In Hard Disk Drive Manufacturing. *J. IEST* **1998**, *41*, 31–35. [CrossRef]
2. Zhang, S.; Wang, L.; Jones, P.; Lopatin, G. Numerical and experimental study of the particle contamination in a head/media interface. *IEEE Trans. Magn.* **1999**, *35*, 2442–2444. [CrossRef]
3. Kasai, P.H.; Raman, V. Hydrocarbon Transfer in Disk Drives. In Proceedings of the 2014 Conference on Information Storage and Processing Systems, ASME International, Santa Clara, CA, USA, 23–24 June 2014.
4. Ambekar, R.P.; Bogy, D.B.; Bhatia, C.S. Lubricant Depletion and Disk-to-Head Lubricant Transfer at the Head-Disk Interface in Hard Disk Drives. *J. Tribol.* **2009**, *131*, 31901. [CrossRef]
5. Ma, Y.; Liu, B. Lubricant transfer from disk to slider in hard disk drives. *Appl. Phys. Lett.* **2007**, *90*, 143516. [CrossRef]
6. Pan, D.; Ovcharenko, A.; Tangaraj, R.; Yang, M.; Talke, F.E. Investigation of Lubricant Transfer between Slider and Disk Using Molecular Dynamics Simulation. *Tribol. Lett.* **2013**, *53*, 373–381. [CrossRef]
7. Mendez, A.R.; Bogy, D.B. Lubricant Flow and Accumulation on the Slider's Air-Bearing Surface in a Hard Disk Drive. *Tribol. Lett.* **2013**, *53*, 469–476. [CrossRef]
8. Marchon, B.; Karis, T.; Dai, Q.; Pit, R. A model for lubricant flow from disk to slider. *IEEE Trans. Magn.* **2003**, *39*, 2447–2449. [CrossRef]
9. Dahl, J.B.; Bogy, D.B. Lubricant Flow and Evaporation Model for Heat-Assisted Magnetic Recording Including Functional End-Group Effects and Thin Film Viscosity. *Tribol. Lett.* **2013**, *52*, 27–45. [CrossRef]
10. Ma, Y.; Liu, B. Dominant Factors in Lubricant Transfer and Accumulation in Slider-Disk Interface. *Tribol. Lett.* **2007**, *29*, 119–127. [CrossRef]
11. Kim, J.-H. Head–disk interface problems in first-surface near-field optical recording with flying optical head. *Curr. Appl. Phys.* **2008**, *8*, 577–582. [CrossRef]
12. Cong, P.; Kubo, T.; Nanao, H.; Minami, I.; Mori, S. Tribological Performance and Transfer Behavior of Lubricating Oils at Head-Disk Interface under Volatile Organic Contamination. *Tribol. Lett.* **2005**, *19*, 299–309. [CrossRef]
13. Sonoda, K. Flying Instability due to Organic Compounds in Hard Disk Drive. *Adv. Tribol.* **2012**, *2012*, 170189. [CrossRef]
14. Seo, Y.W.; Ovcharenko, A.; Talke, F.E. Simulation of Hydrocarbon Oil Contamination at the Head–Disk Interface Using Molecular Dynamics. *Tribol. Lett.* **2016**, *61*, 28. [CrossRef]
15. Wong, D.H.C.; Vitale, A.; Devaux, D.; Taylor, A.; Pandya, A.A.; Hallinan, D.T.; Thelen, J.L.; Mecham, S.J.; Lux, S.F.; Lapides, A.M.; et al. Phase Behavior and Electrochemical Characterization of Blends of Perfluoropolyether, Poly(ethylene glycol), and a Lithium Salt. *Chem. Mater.* **2015**, *27*, 597–603. [CrossRef]
16. Bhushan, B. Magnetic media tribology: State of the art and future challenges. *Wear* **1990**, *136*, 169–197. [CrossRef]
17. Li, L.; Jones, P.; Hsia, Y.-T. Effect of Chemical Structure and Molecular Weight on High-Temperature Stability of Some Fomblin Z-Type Lubricants. *Tribol. Lett.* **2004**, *16*, 21–27. [CrossRef]

18. Mia, S.; Komiya, H.; Hayashi, S.; Morita, S.; Ohno, N.; Obara, S. Viscosity Loss in PFPE Lubricant for Space Applications under EHL Conditions. *Tribol. Online* **2007**, *2*, 54–58. [CrossRef]

19. Morales, W.; Fusaro, R.L.; Siebert, M.; Keith, T.; Jansen, R.; Herrera-Fierro, P. A New Antiwear Additive/Surface Pretreatment for PFPE Liquid Lubricants. *Tribol. Trans.* **1997**, *40*, 321–329. [CrossRef]

20. Jones, W.R., Jr.; Jansen, M.J. *Space Tribology*; NASA/TM-2000-209924; NASA: Washington, DC, USA, 2000.

21. Roberts, E.W. Space tribology: Its role in spacecraft mechanisms. *J. Phys. D Appl. Phys.* **2012**, *45*, 503001. [CrossRef]

22. Weldon, C.A.; Wang, C. Use of PFPE Lubricant in Automotive Applications. US Patent US7608952B2 27 October 2009.

23. Veldhuis, S.; Dosbaeva, G.; Benga, G. Application of ultra-thin fluorine-content lubricating films to reduce tool/workpiece adhesive interaction during thread-cutting operations. *Int. J. Mach. Tools Manuf.* **2007**, *47*, 521–528. [CrossRef]

24. Liu, H.; Bhushan, B. Nanotribological characterization of molecularly thick lubricant films for applications to MEMS/NEMS by AFM. *Ultramicroscopy* **2003**, *97*, 321–340. [CrossRef]

25. Eapen, K.C.; Patton, S.T.; Zabinski, J.S. Lubrication of Microelectromechanical Systems (MEMS) Using Bound and Mobile Phases of Fomblin Zdol®. *Tribol. Lett.* **2002**, *12*, 35–41. [CrossRef]

26. Tani, H.; Iwasaki, K.; Maruyama, Y.; Ota, I.; Tagawa, N. Lubricant Pickup of Ultra-Thin PFPE Lubricants with Different Backbone Structures. *IEEE Trans. Magn.* **2011**, *47*, 1837–1841. [CrossRef]

27. Chung, P.S.; Park, S.; Vemuri, S.H.; Jhon, M.S. Atomistic and Molecular Effects on the Surface Morphology and Film Conformation of Perfluoropolyether Lubricant Layer. *IEEE Trans. Magn.* **2015**, *51*, 1–4.

28. Lotfi, R.; Van Duin, A.C.T.; Biswas, M.M. Molecular Dynamics Simulations of Perfluoropolyether Lubricant Degradation in the Presence of Oxygen, Water, and Oxide Nanoparticles using a ReaxFF Reactive Force Field. *J. Phys. Chem. C* **2018**, *122*, 2684–2695. [CrossRef]

29. Brostow, W.; Hagg Lobland, H.E. *Materials: Introduction and Applications*; John Wiley & Sons: Hoboken, NJ, USA, 2017; ISBN 978-0-470-52379-7.

30. Plimpton, S. Fast Parallel Algorithms for Short-Range Molecular Dynamics. *J. Comput. Phys.* **1995**, *117*, 1–19. [CrossRef]

31. Senftle, T.P.; Hong, S.; Islam, M.; Kylasa, S.B.; Zheng, Y.; Shin, Y.K.; Junkermeier, C.; Engel-Herbert, R.; Janik, M.J.; Aktulga, H.M.; et al. The ReaxFF reactive force-field: Development, applications and future directions. *NPJ Comput. Mater.* **2016**, *2*, 15011. [CrossRef]

32. Chipara, A.; Tsafack, T.; Owuor, P.; Yeon, J.; Junkermeier, C.; van Duin, A.; Bhowmick, S.; Asif, S.; Radhakrishnan, S.; Park, J.; et al. Underwater adhesive using solid–liquid polymer mixes. *Mater. Today Chem.* **2018**, *9*, 149–157. [CrossRef]

33. Srinivasan, S.G.; Van Duin, A.C.T. Molecular-Dynamics-Based Study of the Collisions of Hyperthermal Atomic Oxygen with Graphene Using the ReaxFF Reactive Force Field. *J. Phys. Chem. A* **2011**, *115*, 13269–13280. [CrossRef]

34. Chenoweth, K.; van Duin, A.C.T.; Goddard, W.A. ReaxFF Reactive Force Field for Molecular Dynamics Simulations of Hydrocarbon Oxidation. *J. Phys. Chem. A* **2008**, *112*, 1040–1053. [CrossRef] [PubMed]

35. Kiely, J.D.; Jones, P.M.; Yang, Y.; Brand, J.L.; Anaya-Dufresne, M.; Fletcher, P.C.; Zavaliche, F.; Toivola, Y.; Duda, J.C.; Johnson, M.T. Write-Induced Head Contamination in Heat-Assisted Magnetic Recording. *IEEE Trans. Magn.* **2016**, *53*, 1–7. [CrossRef]

36. Rahman, S.M.; Song, J.; Yeo, C.-D. Computational study on surface energy of amorphous DLC with respect to hybridization state of carbon and potential functions. *Diam. Relat. Mater.* **2019**, *95*, 127–134. [CrossRef]

37. Saito, Y.; Sasaki, N.; Komatsu, T. Molecular Dynamics Simulation for Lubricant Shear Properties During Heating. *IEEE Trans. Magn.* **2011**, *48*, 2009–2015. [CrossRef]

38. Mortier, W.J.; Ghosh, S.K.; Shankar, S. Electronegativity-equalization method for the calculation of atomic charges in molecules. *J. Am. Chem. Soc.* **1986**, *108*, 4315–4320. [CrossRef]